ELSEVIER

Journal of Molecular Catalysis A: Chemical 138 (1999) 249–261

JOURNAL OF MOLECULAR CATALYSIS A: CHEMICAL

Influence of calcination treatment on the structure of grafted WO_x species on titania

A. Scholz [a], B. Schnyder [a], A. Wokaun [b,*]

[a] *Paul Scherrer Institut, CH-5232 Villigen PSI, Switzerland*

[b] *Department of Chemical Engineering and Industrial Chemistry, Swiss Federal Institute of Technology, ETH Zentrum, CH-8092 Zürich, Switzerland*

Received 6 August 1997; accepted 29 April 1998

Abstract

TiO_2/WO_x supported metal oxide materials were prepared by grafting a tungsten(V)ethoxide precursor onto a titania support. The supported metal oxides were characterized by Raman spectroscopy under ambient conditions in oxygen and inert gas atmosphere. Measured under ambient conditions, the samples are sensitive to a variation in laser power. This effect is a function of the tungsten loading. During calcination of the samples in either inert gas atmosphere (N_2) or oxidizing atmosphere (O_2), this sensitivity is not observed. After cooling the samples to room temperature under inert gas conditions, a sensitivity of the surface structures to a laser power variation is again recorded. The structural changes are due to thermal effects and not to an adsorption of water. The composite band structure in the Raman spectra of the samples leads to the conclusion that octahedrally and tetrahedrally coordinated WO_x surface structures as well as polytungstates are co-existing on the surface, and are forming cross linked structures. According to the XPS data, the structure of the metal oxide species depends on the monolayer coverage on the support.

Keywords: Raman spectroscopy; XPS; WO_x species

1. Introduction

Several methods for the preparation of supported metal oxide catalysts have been reported in the literature. The techniques of aqueous impregnation and incipient wetness using the salts of metal complexes have been described by various authors [1–9]. Another preparation method is solid–solid wetting which is described by Leyrer at al. [10] and authors cited therein. Grafting of metal alkoxide precursors onto a metal oxide support alkoxides results in highly dispersed metal oxide species on the carrier. The preparation of vanadia layers on TiO_2 using vanadyl alkoxides $VO(OR_3)$ has been reported, e.g., by Baiker et al. [11,12], Schraml et al. [13], and Handy et al. [14]; grafting of vanadia onto other supports was also considered [15]. Grafting a TiO_2 support with tungsten(V)ethoxide was first described by Engweiler and Baiker [16].

In this work, we investigated the surface structure of grafted tungsten oxide catalysts by Raman spectroscopy. We focused our attention on the spectral changes in the vibrational modes of the WO_x surface species as a function of the

* Corresponding author.

1381-1169/99/$ - see front matter
PII: S1381-1169(98)00162-9

number of grafting steps and the calcination treatment under ambient conditions and under inert gas atmosphere. The amount of tungsten and its oxidation state was determined by XPS. Moreover, we tried to find out whether a variation of laser power gives rise to reversible band shifts in the W=O stretching frequency region, or whether laser crystallization of WO_3 species can be observed.

The characterization of supported metal oxides with Raman spectroscopy is a useful method for identifying surface oxide groups. Stencel [17] has reviewed this method in detail. Based on the symmetry of tungsten oxide species in solution and in the solid state, it is possible to assign the following classes of structural units for tungsten oxides: (1) tetrahedrally coordinated units of type WO_4, (2) octahedrally coordinated complexes of the type WO_6, (3) W–O–W bonds, and (4) lattice modes. A survey of these vibrational modes and their Raman frequencies is given in Refs. [18–20]. Horsley et al. [4] have investigated the structure of WO_x supported on Al_2O_3 by Raman spectroscopy. Surface tungsten oxide species are strongly bound on the support surface as was shown by Chan et al. [3].

TiO_2 shows strong anatase Raman bands at 520, 643, and 399 cm^{-1} [17,21]. Those features make the detection of tungsten oxide vibrational frequencies in this region difficult. At 794 cm^{-1}, a weak second order feature of anatase is found, which can be easily distinguished from the sharp peak of crystalline WO_3 at 804 cm^{-1}. For identification of the tungsten oxide species on the support, the W=O stretching frequencies of octahedral tungsten oxide units in the range from 740 to 980 cm^{-1}, and the W=O stretching frequencies of the tungsten–oxygen tetrahedral units between 913 and 1060 cm^{-1} have to be recorded. The stronger Raman signal from tetrahedral structures of surface tungsten oxides is due to their higher W–O bond order compared to the octahedral structures. Thus, the Raman spectrum of samples possessing both structures will be dominated by bands assigned to tungsten oxide tetrahedra [4]. The effect of laser power on sample spectra has not very often been discussed in literature. Payen et al. [22] mentioned reversible spectral changes induced by a variation of laser power (20–40 mW to 150–200 mW) for a MoO_3–γ-Al_2O_3 catalyst. The authors observed a reversible line shift of the Mo=O vibrational frequency. No transformation of supported polymolybdate into crystalline MoO_3 was observed. This was associated with local heating of the sample which results in a calcination in air. Thermal influence on the symmetrical (W=O) stretching mode due to heating of a 7% WO_3/TiO_2 sample in an in situ cell is reported by Chan et al. [23]. The authors observed a sharpening and shift of the Raman feature at 966 cm^{-1} when the sample was heated to 873 K. After cooling the sample to 453 K, the sharp and shifted feature remained. The exposure of the sample to an ambient air atmosphere for 12 h restored the previous spectrum. Their conclusion was that the band shift is not due to thermal effects but to desorption and adsorption of water vapor on the sample.

The oxidation states of supported metal oxides and the amount of metal at the support can be determined by X-ray photoelectron spectroscopy (XPS). This technique was used for example for chromium on different supports [24] and for tungsten supported on Al_2O_3 and TiO_2 [25,26].

2. Experimental

2.1. Sample preparation

The TiO_2/WO_3 samples were prepared by a multi-step grafting procedure which is analogous to the one described in detail in Ref. [27]. TiO_2 (P25, Degussa) was stirred with distilled water, dried at 493 K overnight and ground with a mortar and pestle. The alkoxide precursor, tungsten(V)ethoxide (ABCR, purity grade 95%) was dissolved in *n*-hexane (Fluka, p.a.) dried

over molecular sieve. All grafting steps were carried out under an inert atmosphere of Ar. Samples with one to four grafted layers were prepared and labeled as *x*WTi, where *x* is the number of grafting steps. After each grafting step, the excess amount of precursor solution was removed by washing the sample three times with fresh solvent. Then the sample was dried under vacuum (10^{-1} mbar) for 24 h. No calcination between grafting steps was performed as described in Ref. [27]. Some uncalcined material of the third and fourth grafting step was stored separately. After the final grafting step, samples were calcined under a constant N_2 flux for 3 h at 573 K.

2.2. Raman measurements

The Raman measurements were carried out on a confocal Raman microscope (Labram, DILOR) equipped with an HeNe laser (632.8 nm) and a Peltier cooled CCD camera. The pinhole aperture was set to 500 μm. For all measurements, an ultra long working distance objective (Olympus, 50$\times$ magnification) was used. The spectral resolution was set to 4 cm^{-1}. Laser power was attenuated with a neutral density filter (NG3, Schott). The laser power focused onto the sample was 2.5 mW for high laser power applications and 0.26 mW for low laser power applications. Three spectra were measured for each sample, first at low power, second at high power, and finally again at low laser power. The interval without laser illumination between each measurement was approximately 2 s, the time necessary to change the neutral density filter.

Measurements of the samples exposed to air at room temperature (referred to here as ambient conditions) were carried out by placing the uncalcined sample on a microscope slide and slightly pressing it to obtain a planar surface. The collection time per spectrum was 40 s, and five spectra were co-added. The measurements in an inert atmosphere were performed with a Linkam TMS 1500 heatable microscope stage under constant N_2 or O_2 flow (60 ml/min). The stage permits the control of the environmental conditions before and during data acquisition. The sample was placed in the sample holder and was slightly pressed to obtain a planar surface. Then, the temperature was ramped consecutively at 10 K/min to 573, 673, 773, 873, 973, and finally 1073 K. At each temperature, the sample was held for 1800 s. After 600 s of thermal equilibration, the Raman spectra were collected. For each spectrum, the collection time was 20 s per spectrum and 10 spectra were accumulated.

2.3. Analysis of the spectra

In the region of interest where the WO_x vibrational frequencies are found (860 to 1050 cm^{-1}), the spectra show an intense background arising from the TiO_2 support. A background correction was achieved by fitting a fourth-order polynomial to the data set and then subtracting it, according to Went et al. [28].

In order to compare the spectra measured with low laser power to those recorded with high laser power, the intensity of the high laser power spectra were multiplied by the filter transmission coefficient (0.104). Between 860 and 1050 cm^{-1}, the spectra contain contributions of tetrahedrally and octahedrally coordinated tungsten oxide species whose bands overlap. The composite bands were separated into contributions from individual tungsten oxide species using a commercial peak fitting routine (Lab Calc, Galactic Instruments). Prior to the fit, the composite band profile was differentiated in order to determine the appropriate *number* of component peaks. The quality of the fit was judged by the mean square deviation χ^2, and from the agreement of fitted line widths with literature values.

2.4. XPS measurements

XPS measurements have been performed on a ESCALAB 220i XL instrument (VG Scien-

tific). The photoelectron spectrometer was equipped with an aluminium anode X-ray source ($h\nu = 1486.6$ eV) which was operated at a power of 300 W (15 kV, 20 mA). Vacuum in the analysis chamber was better than $5 \cdot 10^{-9}$ mbar. For the measurements, the instrument was operated in the constant analyzer energy (CAE) mode at a resolution of 1 eV. Binding energy values were referenced to the C 1s (284.6 eV), and Ti 2p 3/2 (458.7 eV) signals [29]. For the measurements, the sample material was pressed into pellets. To quantify the atomic concentration of the present elements, the cross sections according to Scofield [30] have been used.

3. Results

3.1. XPS measurements

Two energy levels of tungsten have been measured in the W 4d and the W 4f region. The W 4d peak is broad and cannot be used to determine the oxidation state, but it is useful to quantify the amount of tungsten on the support. Analysis of the W 4f region is complicated by interference from the Ti 3p level of the support, especially when tungsten is highly oxidized, i.e., when it has a high binding energy. By curve fitting it was possible to distinguish between the two signals, see Fig. 1. Peak position and peak width of the Ti 3p band was determined by curve fitting of a TiO_2 reference sample. So it was possible to separate the two contributions properly, and to determine the valence of the tungsten from the position of the W 4f level, for which many reference data are available. The measured spectra appeared similar for all samples, and showed identical positions for the W 4f peaks. Only minor charging was observed and corrected. The following binding energies are observed. Ti 2p 3/2: 458.7 eV; Ti 3p: 36.9 eV; W 4f 7/2: 35.1 eV; O 1s: 530.0 eV. The O 1s binding energy corresponds well with reference data [29] for the O 1s level

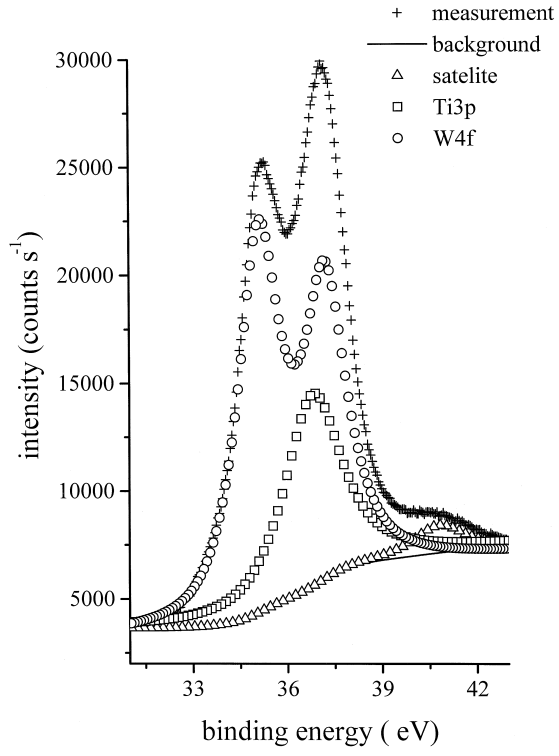

Fig. 1. XPS spectrum of the Ti 3p/W 4f region of sample 4WTi.

of TiO_2 (529.9 eV). The slightly higher energy can be explained by the presence of oxidized tungsten species which are present in small quantities and have slightly higher binding energies (WO_2: 530.4 eV; WO_3: 530.6 eV [30]). For the W 4f 7/2 level, we find a constant position of 35.1 eV, which does not match exactly the value for WO_3 (35.8 eV), or even less the binding energy of WO_2 (32.8 eV) given in [29]. Fiedor et al. [26] found for a W/TiO_2 system, which was prepared with another preparation method, a binding energy of 35.5 eV for W 4f 7/2 and of 37.3 eV for Ti 3p. Both binding energies are 0.4 eV higher than the binding energies measured in this investigation. This may be due to a systematic error. The authors assigned their peak position to W^{6+} of WO_3, as we do in the present investigation. Only W^{6+} centers were detected. The differences between the binding energies of the literature reference samples and those found in our present investi-

Table 1
XPS measurements of WO_x/TiO_2

	W content (at.%)	O/Ti	W/Ti	Monolayer coverage
TiO_2	0.0	2.23	0.00	–
3WTi[a]	3.80	2.83	0.18	1.11
4WTi[a]	4.60	2.58	0.21	1.29
1WTi[b]	2.50	2.72	0.12	0.78
2WTi[b]	2.90	2.61	0.13	0.85
3WTi[b]	4.40	2.97	0.22	1.32
4WTi[b]	3.60	2.91	0.18	1.13

[a]Uncalcined samples.
[b]Calcined samples (in N_2 at 973 K).

gation can be explained by the presence of TiO_2 in the neighborhood of the tungsten centers. Our samples contain a relatively small amount of tungsten on the TiO_2 surface, see Table 1. For the two uncalcined samples, the amount of tungsten deposited has been confirmed by independent atomic absorption spectroscopy (AAS) measurements. Consequently, most of the tungsten is bound to TiO_2 and forms a compound with a characteristic binding energy, analogous the compound $CaWO_4$ with a binding energy of 35.0 eV [29]. It should also be mentioned that some non-stoichiometric tungsten oxides exist such as $W_{20}O_{58}$, $W_{18}O_{49}$, $W_{50}O_{148}$ and $W_{40}O_{119}$. Only for $W_{18}O_{49}$ a value of the binding energy (34.3 eV) is recorded in Ref. [29], which is again lower than our measured values.

3.2. The TiO_2 support

At room temperature, the TiO_2 support shows the major anatase bands and a weak rutile peak at 448 cm^{-1}, as has been reported for P25 in the literature [21]. With heating of the samples, the rutile peak vanishes as the anatase bands broaden, as has been reported by Chan et al. [23]. Cooling the samples down to room temperature restores the rutile peak again. The calcination temperature in this investigation was chosen to be always less than 1170 K, the point were the anatase-to-rutile transformation in the presence of WO_3 takes place [31,32].

3.3. Uncalcined samples

The samples 3WTi and 4WTi were measured under ambient conditions (a) first with low laser power, (b) with high laser power, and (c) finally with low laser power. In Figs. 2 and 3, the region between 860 and 1050 cm^{-1} where the tungsten oxide species can be detected is shown. The sample 3WTi (Fig. 2) exposed to the experimental sequence described above is not influenced by laser power variation. The peak maximum remains at $\sim$960 cm^{-1}. For 4WTi (Fig. 3) trace (a) consists of a broad band between 900 and 1000 cm^{-1} with its maximum at $\sim$950 cm^{-1}. The application of high laser power broadens this band and shifts its maximum to $\sim$980 cm^{-1} with a steep decline towards 1000

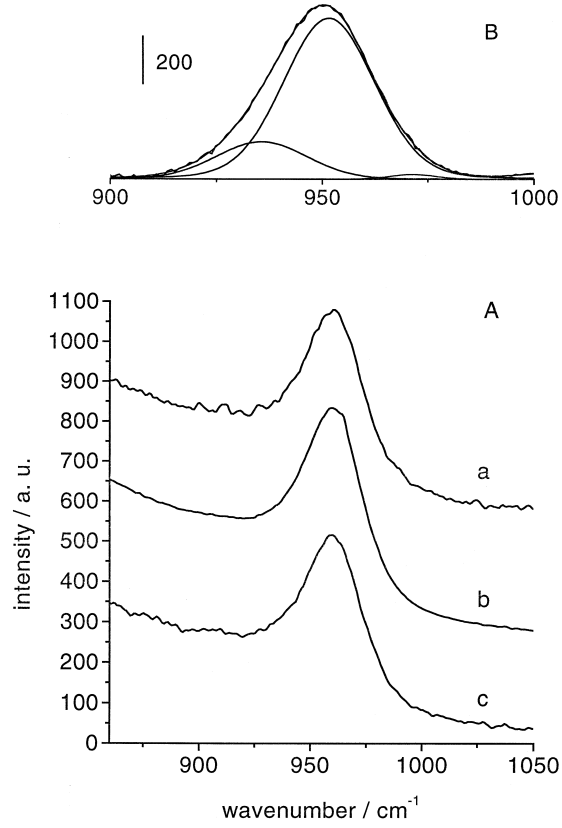

Fig. 2. Raman spectra of sample 3WTi (uncalcined), measured in sequence with low (a), high (b), and low (c) laser power, part (A). As an example, part (B) shows a fit of the baseline corrected spectrum recorded using high laser power.

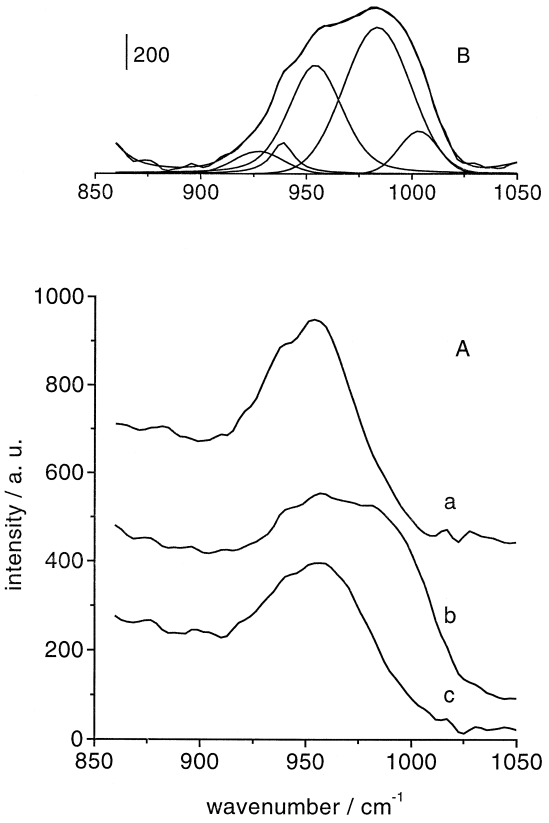

Fig. 3. Raman spectra of sample 4WTi (uncalcined), measured in sequence with low (a), high (b), and low (c) laser power, part (A). As an example, part (B) shows a fit of the baseline corrected spectrum recorded using high laser power.

cm^{-1}, trace (b). Applying low laser power again, trace (c), the original band structure is restored, indicating a reversible structural change in the sample. The band maximum is again found at ~950 to 960 cm^{-1}. Comparing Figs. 2 and 3 shows that the spectra of the 4WTi sample exhibit a more complex and broad W=O stretching band than those of the 3WTi samples.

3.4. Calcined samples

All spectra were recorded under a constant gas flow of either N_2 or O_2 providing an inert gas or an oxidizing atmosphere. Each sample was measured as described in Section 2. The spectra were recorded always at the same spot in order to find out whether a variation of laser power would give rise to the same band shift as for the uncalcined samples. Laser damage could be ruled out by visual inspection of the sample surface. The measurements of the N_2 calcined samples demonstrated that upon increasing the calcination temperature, the changes of band position and band shape, as described for 3WTi at ambient conditions, become less significant and vanish completely for calcination temperatures above 673 K. The O_2 calcined samples displayed no laser induced changes at any temperature.

The initial low laser power spectra of the samples which were treated in an inert gas atmosphere (N_2) at the lowest calcinations temperature of 573 K showed the following characteristics. For every grafting step, a strong background, less pronounced TiO_2 bands, and no species of WO_x in the W=O stretching region could be detected. This behaviour is shown in Fig. 4 (trace (a)) for 1WTi. After the application of high laser power, the TiO_2 bands (not shown)

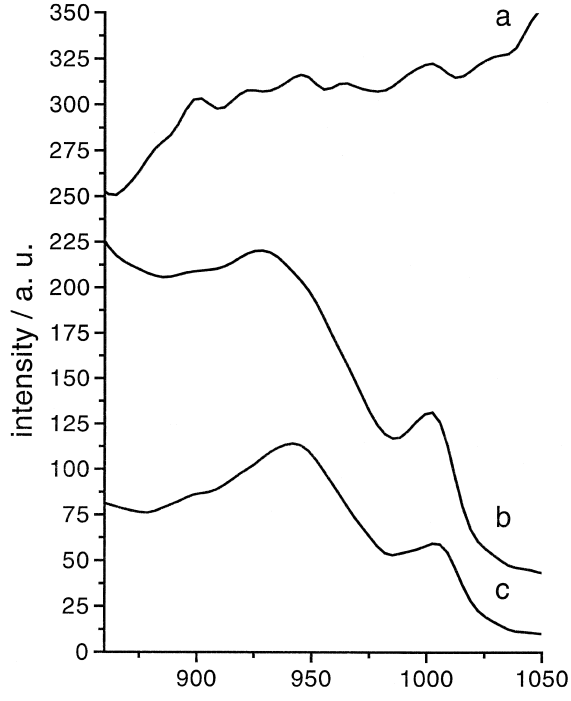

Fig. 4. Raman spectra of sample 3WTi at 573 K, N_2, measured in sequence with low (a), high (b), and low (c) laser power.

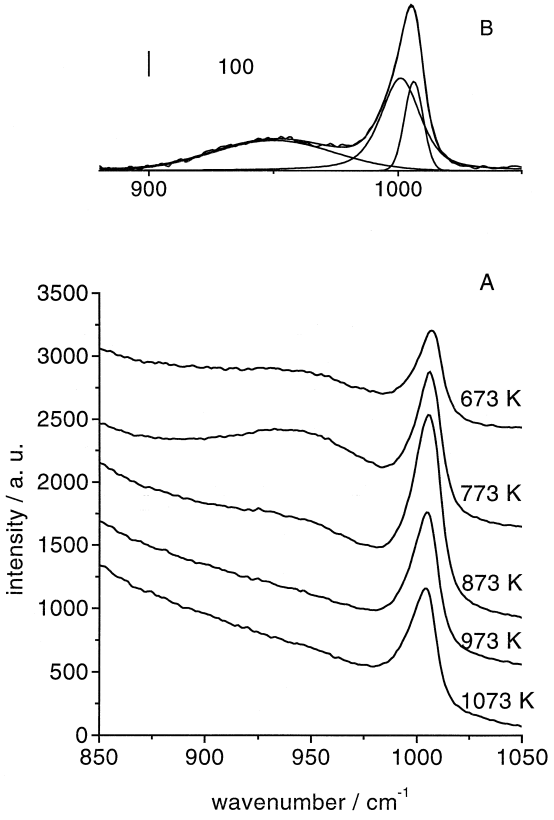

Fig. 5. Raman spectra of sample 2WTi measured during calcination in N_2 at temperatures increasing from 673 to 1073 K, part (A). As an example, part (B) shows a fit of the baseline corrected spectrum at 773 K.

and WO_x bands (860 to 1050 cm^{-1}) become more intense, Fig. 4 (trace (b)). Trace (c) (low laser power) shows no significant difference with respect to the TiO_2 and WO_x band structure.

Increasing the calcination temperature to $\geq$ 673 K, the samples showed distinct TiO_2 and WO_x features for all measurements. The WO_x band profile consist of two parts, a broad band between $\sim$900 and $\sim$975 cm^{-1} and a relatively sharp peak at $\sim$1000 cm^{-1}, as can be seen in Fig. 5. The form and intensity of these two features depend on calcination temperature and tungsten loading. Regarding the intensity ratio of broad band and sharp peak, the samples can be divided in two groups. First, samples with low tungsten loading (1WTi, 2WTi). For these, the broad band is less intense than the peak. Increasing the calcination temperature causes an intensity increase for the band up to a temperature of 773 K. Further temperature increase causes an intensity decrease of this band, as shown for 2WTi in Fig. 5. Second, samples with high tungsten loading (3WTi, 4WTi). For the latter samples, the contribution of the broad band dominates the spectra. The intensity of this band decreases with a temperature increase, see Fig. 6.

After cooling the samples to room temperature still under inert gas atmosphere another series of spectra with varying laser power was recorded. In Fig. 7, the spectra of sample 4WTi are presented. It was found that the peak at

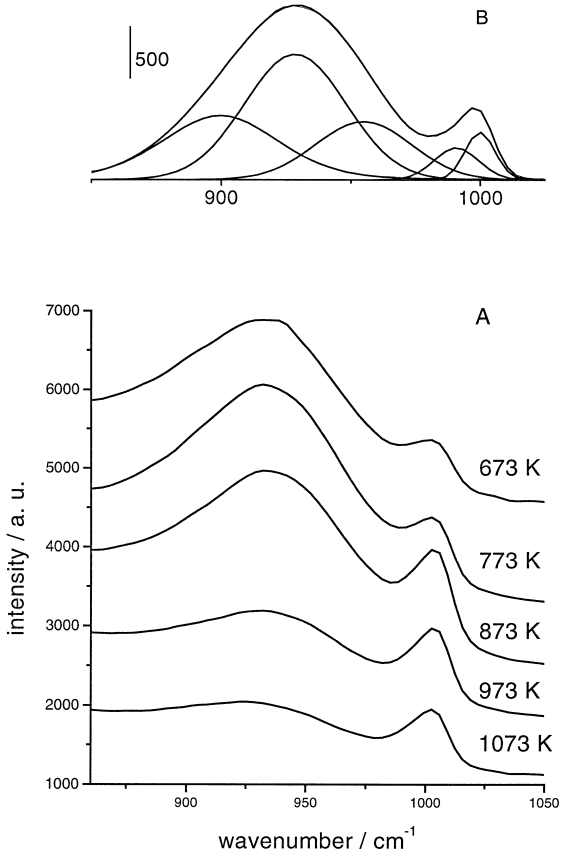

Fig. 6. Raman spectra of sample 3WTi measured during calcination in N_2 at temperatures increasing from 673 to 1073 K, part (A). As an example, part (B) shows a fit of the baseline corrected spectrum at 873 K.

$\sim 1000\ cm^{-1}$ had nearly vanished. Besides, the samples are to some extent sensitive to a variation of laser power again.

Calcination of the samples in an oxidizing atmosphere (O_2) changes the Raman spectra drastically compared to a treatment in N_2 gas atmosphere. The initial low laser power spectrum at 573 K shows distinct TiO_2 and WO_x bands. For all calcination temperatures and grafting steps the spectra are dominated by a peak with its maximum at $\sim 1008\ cm^{-1}$ for 1WTi and 2WTi and at $\sim 990\ cm^{-1}$ for 3WTi and 4WTi. The broad band (~ 900 to $\sim 975\ cm^{-1}$) which was observed for the N_2 calcined samples is diminished into a shoulder of the main peak. With increasing temperature, this shoulder vanishes and no broad band can be detected, see Fig. 8. After cooling the samples to room temperature under oxygen, the band shape changes. The dominating peak vanishes and is replaced by a broad feature between 900 and $\sim 1000\ cm^{-1}$, similar to the one observed for the N_2 calcined samples. The spectra show no sensitivity to a variation of laser power.

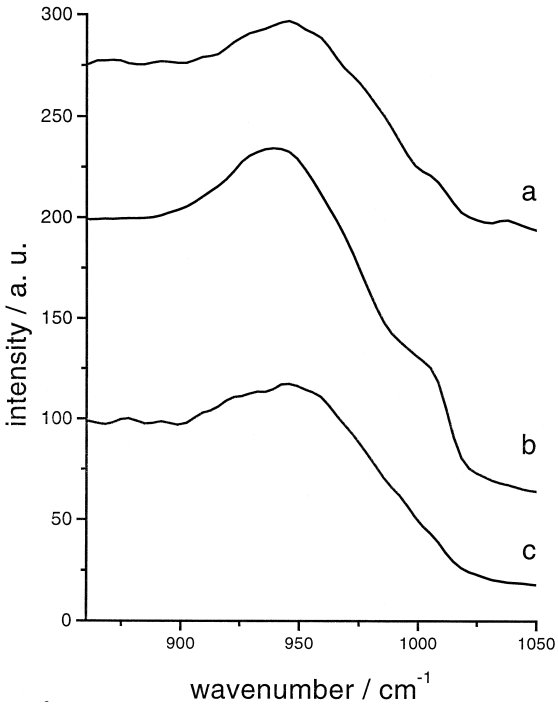

Fig. 7. Raman spectra of sample 4WTi after calcination at 1073 K in N_2. The spectrum was subsequently measured after cooling to room temperature in N_2 atmosphere using low (a), high (b), and low (c) laser power.

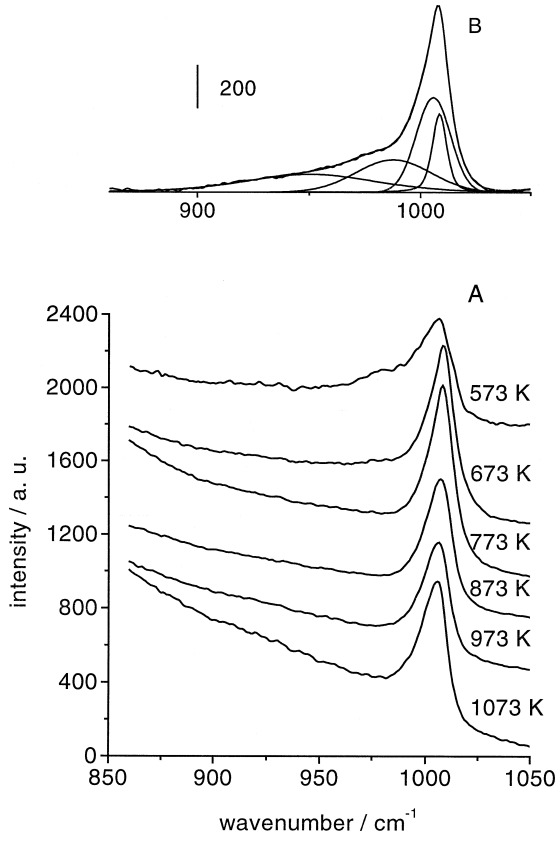

Fig. 8. Raman spectra of sample 2WTi measured during calcination in O_2 at temperatures increasing from 573 to 1073 K, part (A). As an example, part (B) shows a fit of the baseline corrected spectrum at 773 K.

4. Discussion

4.1. Amount of tungsten on the support (XPS)

As can be seen in Table 1, the tungsten concentration does not increase linearly from the first to the fourth grafting step for the calcined samples. On sample 3WTi more tungsten has been deposited on the support than after four grafting steps. This is probably an effect of evaporation during calcination. Calculating the monolayer coverage of WO_x species

on the TiO_2 surface shows that for the third and fourth grafting step, more than one monolayer of tungsten oxide species were deposited, see Table 1. The calculation of the monolayer coverage was performed according to the procedure of Seah [33] with an average free path length calculated according to Ref. [34] ($\lambda_{(W)} = 18.1$ Å, $\lambda_{(Ti)} = 15.6$ Å). The model of Bond et al. [35] which suggests that a fraction of the surface of the support is covered by towers consisting of disordered and paracrystalline metal oxide was not used, because in this investigation, no crystalline WO_3 species were detected.

4.2. Raman spectra of the uncalcined samples (3WTi / 4WTi)

The structure and complexity of the spectra in the region of the WO_x stretching frequencies provides some information on the number of distorted WO_x species at the surface. The most important peaks with strong and medium intensity resulting from applying a peak fitting routine to the spectra are thought to represent actual WO_x species at the support, whereas the weak features provide only confirming information.

The peak positions of the curve fitted spectra of uncalcined samples in the region from 860 to 1050 cm^{-1} are listed in Table 2. The spectra of the 3WTi samples were best fitted with two to three peaks, compare Fig. 2. For all laser intensities, the largest peak lies at ~ 950 cm^{-1}. With high laser power, the peak splits into two components. One remains at 952 cm^{-1} and the other shifts to 971 cm^{-1}. Remarkably, no peaks that could be exclusively assigned to tetrahedral species were detected. The spectra of 4WTi were modeled with five peaks, compare Fig. 3. Between 913 and 980 cm^{-1} bands due to octahedrally and tetrahedrally coordinated W centers overlap. However, peaks above and below these limits can be unambiguously assigned [4]. The peak positions for high and low laser power applications are similar within the spectral resolution for the first three peaks (920–927, 937–939, and 954–956 cm^{-1}). The major peak is always located at 954–956 cm^{-1}. Increasing the laser power causes the peaks at 969 and 987 cm^{-1} to shift to 984 and 1003 cm^{-1}. The peak at 1003 cm^{-1} also increases in intensity. Lowering the laser power shifts the peak positions back to 975 and 996 cm^{-1} while the latter peak decreases in intensity. The peaks at 984 and 1003 cm^{-1} can be unambiguously assigned to a tetrahedrally coordinated WO_x species. The weak peaks (987 and 996 cm^{-1}) are an indication that even for the application of low laser power, a few of these tetrahedrally coordinated W centers may exist. The changes suggest that with the application of high laser power, new tetrahedrally coordinated tungsten oxide species are formed. The band shifts with varying laser power (Table 2), i.e., from 969 to 984 cm^{-1} ($\Delta = 15$ cm^{-1}) and back to 975 cm^{-1} ($\Delta = -9$ cm^{-1}), and from 987 to 1003 cm^{-1} ($\Delta = 16$ cm^{-1}) and back to 996 cm^{-1} ($\Delta = -7$ cm^{-1}), are remarkably lower than the results of Chan et al. [23] who detected a band shift of the symmetric Mo=O stretch of ~ 30 to 40 cm^{-1} upon heating (873 K). The smaller shift in the present work is possibly the result of a lower temperature change induced by the laser in the case of WO_x/TiO_2.

Table 2
Fitted peak positions in the spectra of the uncalcined samples 3WTi (Fig. 2) and 4WTi (Fig. 3)

Sample	Peak position/cm^{-1}	Laser power
4WTi	920(w)/937(s)/954(s)/969(s)/987(w)	low (trace (a))
	927(m)/939(w)/954(s)/984(s)/1003(m)	high (trace (b))
	923(w)/938(m)/956(s)/975(m)/996(w)	low (trace (c))
3WTi	924(w)/950(s)	low (trace (a))
	936(m)/952(s)/971(w)	high (trace (b))
	924(w)/950(s)	low (trace (c))

4.3. Raman spectra of the calcined samples

4.3.1. N_2 inert gas atmosphere

The spectra of the samples show two features in the region between 850 and 1050 cm^{-1}, a broad band between 900 and ~ 980 cm^{-1} and a

sharp peak at ~1000 cm^{-1}. The broad band was best modeled with one peak for 1WTi and 2WTi and with four to five peaks for 3WTi and 4WTi according to an increasingly complex band shape, compare Figs. 5 and 6. The peak at ~1000 cm^{-1} was best fitted with two peaks for all samples. With increasing tungsten oxide loading the intensity of the broad band increases compared to the intensity of the peak.

4.3.2. O_2 gas atmosphere

The spectra of the samples show a weak band around 950 cm^{-1} and an intense and sharp peak at ~1000 cm^{-1} for 1WTi and 2WTi, and between 988 and 994 cm^{-1} for 3WTi and 4WTi. This peak is best modeled by two to three peaks. An increase in tungsten oxide loading leads to a decrease in the intensity of the broad band compared to the peak. Additionally, the spectra become less complex, contrary to the results obtained after a calcination in an N_2 atmosphere. The broad band is best modeled with three to five peaks for 1WTi, whereby the number of deconvolution peaks decreases with increasing calcination temperature. For 2WTi, 3WTi, and 4WTi, the broad band is best modeled with two bands, compare Fig. 8.

4.4. Peak assignment

An assignment of octahedral WO_3 modes (below 913 cm^{-1} [4]) is possible for the highly grafted N_2 calcined samples. O_2 calcined samples show practically no modes of octahedrally coordinated WO_x species. The peak distribution depending on calcination temperature is shown in Table 3. After the third and fourth grafting step, the N_2 calcined samples show a significant change in their spectra. The spectra are of a more complex structure. The octahedrally coordinated WO_x modes are roughly located around 900 cm^{-1}.

Peaks over 980 cm^{-1} can be exclusively related to tetrahedrally coordinated WO_x species [4]. The peak positions obtained from the fitted spectra for four representative samples are shown in Table 4. Most spectra exhibit two spectral features above 980 cm^{-1}. The peak positions resulting from the peak fitting are not altered by increasing the calcination temperature. Increasing the tungsten loading, however, shifts the peak positions to lower frequencies (by 6 to 18 cm^{-1}) as can be seen for the N_2 calcined samples and as well for the O_2 calcined samples. Further, the band positions of the O_2 calcined samples are located at lower frequencies compared to the N_2 samples (by 5 to 10 wavenumbers).

The peak distribution of the spectra after N_2 calcination agrees with the results of Vuurman et al. [36] who found tetrahedrally coordinated tungsten oxide species at low loadings and octahedrally coordinated tungsten oxide species at moderate loadings under ambient conditions. In consideration of the XPS results, we can state that tetrahedrally coordinated WO_x species are found below one monolayer coverage. Above one monolayer also octahedrally coordinated WO_x species are present. Heating in an inert gas

Table 3
Fitted peak positions of octahedrally coordinated WO_x species

Calcination temperature (K) / Sample	573	673	773	873	973	1073	
	Peak position/cm^{-1}						Calcination atmosphere
1WTi/2WTi	–	–	–	–	–	–	N_2
3WTi	912	896	900	890	–	–	
4WTi	898	–	890/904	898	901	896	
1WTi	909	911	–	–	–	–	O_2
2WTi/3WTi/4WTi	–	–	–	–	–	–	

Table 4
Fitted peak positions of tetrahedrally coordinated WO_x species

Calcination temperature (K) Sample	573	673	773	873	973	1073	
	Peak position/cm^{-1}						Calcination atmosphere
1WTi		998	999	999	995	995	N_2
	1003	1005	1005	1004	1002	1001	
4WTi	995	980	991	987	998	991	
	1001	997	999	996	998	999	
1WTi	991(m)	995(m)	994(m)	995(s)	997(s)	990(m)	O_2
	1002(s)	1004(s)	1004(s)	1003(s)	1004(s)	1002(s)	
					1019(w)	*1023(w)*	
4WTi	986	982	982/989	990	986	977	
	–	990	991	1003	994	986	

atmosphere does not change the structure of the tungsten oxide surface species compared to ambient conditions.

The increasing intensity of the broad band in the spectra with increasing tungsten loading suggests that a number of isolated octahedrally and tetrahedrally coordinated WO_x species coexist with polytungstate species. The latter species are represented by a broad band around 960 cm^{-1} according to Vuurman et al. [36]. The stretching modes of the polytungstates were assigned by analogy with the vibrational modes of solvated species like $W_6O_{10}(OH)^{5-}$(aq), $W_{12}O_{39}^{6-}$(aq), or $W_{12}O_{41}^{10-}$(aq), which all have a distorted octahedral coordination [37]. The simulation of the spectra of the samples 1WTi and 2WTi calcined in N_2 exhibits one polytungstate peak around 941 to 950 cm^{-1}. The spectra of the samples 3WTi and 4WTi exhibit two peaks between 926 and 958 cm^{-1}.

The shift to lower wavenumbers of vibrational frequencies of tetrahedrally coordinated species with increasing tungsten loading indicates that the terminal W=O bond increases in length. It may be influenced by an increasing number of differently distorted, surrounding octahedrally coordinated WO_x surface species. The samples exposed to an O_2 atmosphere show polytungstate species in their spectra after every grafting step. For the spectra of 1WTi, two to three polytungstate peaks are located between $\sim$920 to 960 cm^{-1}. With higher tungsten loading only one polytungstate peak remains which is located at $\sim$950 cm^{-1}. With increasing the calcination temperature, the peak intensity of the polytungstate vibrational modes decreases. This indicates that isolated tetrahedrally coordinated species are the dominating WO_x surface species.

To model the band structure of the samples which were cooled down under in situ conditions, a large number of composite bands was required. It is interesting that the high wavenumber features $\geq$1000 cm^{-1} still exist in the spectra recorded with low laser intensity, compare Fig. 7. This means that cooling the samples does not completely change the surface oxide structure that is established upon heating, but instead causes a depletion of isolated tetrahedral species in favour of polytungstate structures. Although the O_2 calcined samples show a low intensity of the polytungstate band while heating, this band dominates their spectra after cooling. Variation of laser power showed that the N_2 calcined samples are still sensitive to a change in laser power. As can be seen in Fig. 7, the intensity of the band at 1006 cm^{-1} increases with increasing laser power (trace (b)). At low laser power, the spectra (traces (a) and (c)) exhibit a shoulder on the high wavenumber side, which was modeled using a peak at 972 cm^{-1}. The number of peaks necessary for the

spectral simulation decreases with increasing laser power. Laser heating of the sample brings about an increase in the intensity of the bands due to isolated tetrahedrally coordinated species, whereas with low laser power, the signal of the polytungstate species are the dominant feature. The O_2 calcined samples show no dependence on variation in laser power. The spectral changes with heating and with varying laser power indicate that the structure of the surface species depends on the temperature of the sample, and is reversible. From the present data, no information on the formation of W/Ti mixed oxides can be derived.

As reported by Chan et al. [38] for the WO_3/Al_2O_3 system at low coverages, tungsten oxide is in a highly dispersed and amorphous state on the alumina surface. This is in agreement to the spectra measured in N_2 at 573 K (Fig. 2). With increasing calcination temperature the WO_x species disperse over the surface and form octahedrally, tetrahedrally coordinated, and polytungstate species. A significant peak shift can be recognized with increasing tungsten oxide loading. The more tungsten oxide is present at the surface, the less isolated tetrahedral WO_x species can be detected. This suggests that the tungsten oxide species are highly dispersed at low coverages and form cross linked octahedral and tetrahedral WO_x structures at higher coverages.

5. Conclusions

In this study, the WO_x/TiO_2 system derived from a tungsten(V)ethoxide precursor was characterized by Raman spectroscopy under inert gas (N_2) and under oxidizing conditions as well as under ambient conditions. The applied laser power was varied in order to determine the influence of the laser intensity on the vibrational modes of the WO_x surface species. From XPS measurements, the amount of tungsten on the support and its oxidation state were determined. On all samples, tungsten is in its W^{6+} state. The decrease in tungsten content for the calcined samples shows that a thermal treatment may influence the tungsten at the support. For the third and fourth grafting step more than monolayer coverage of tungsten oxide species on the support was achieved. The Raman measurements of the uncalcined samples showed that laser induced structural changes of the WO_x species depend on the amount of tungsten loading.

The Raman spectra of the samples show substantial differences between the different calcination treatments in either N_2 or O_2 atmosphere. Calcining the samples in an N_2 atmosphere results in spectra of a complex band shape dominated by an intense broad band between 950 and 975 cm^{-1}, which is assigned to polytungstates. The spectra of the samples calcined in an oxidizing atmosphere do not show such an intense broad band. They are dominated by a sharp peak at 990 cm^{-1} assigned to tetrahedral species. With increasing calcination temperature, the samples calcined in N_2 and O_2 atmosphere are not affected by a variation of laser power. This implies a stable, temperature-dependent distribution of highly dispersed WO_x species which is created during high temperature calcination. With increasing tungsten loading octahedrally and tetrahedrally coordinated structures, as well polytungstates, are found. The structure of the surface species can be related to the monolayer coverage on the support. With more than one monolayer coverage on the support octahedrally coordinated WO_x species are formed.

Cooling the samples to room temperature in situ after calcination changes their spectra completely. The signals due to polytungstates become much more intense, whereas the peaks of the tetrahedrally coordinated species decrease in intensity but remain observable. The fact that these changes are taking place while the samples are exposed to a dry N_2 or O_2 atmosphere indicates that the induced structural changes are due to thermal effects rather than to adsorption of water.

Acknowledgements

The authors thank Mr. Keil for providing supporting AAS measurements.

References

[1] T. Yamaguchi, S. Nakamura, K. Tanabe, J. Chem. Soc., Chem. Commun. (1982) 621.
[2] J.M. Stencel, L.E. Makovsky, J.R. Diehl, T.A. Sarkus, J. Raman Spectrosc. 15 (1984) 282.
[3] S.S. Chan, I.E. Wachs, L.L. Murrell, J. Catal. 90 (1984) 150.
[4] J.A. Horsley, I.E. Wachs, J.M. Brown, G.H. Via, F.D. Hardcastle, J. Phys. Chem. 91 (1987) 4014.
[5] S.L. Soled, G.B. McVicker, L.L. Murrell, L.G. Sherman, N.C. Dispenziere Jr., S.L. Hsu, D. Waldman, J. Catal. 111 (1988) 286.
[6] C.U.I. Odebrand, A. Bahamonde, P. Avilar, J. Blanco, Appl. Catal. B 5 (1994) 117.
[7] P. Patrono, A. La Ginestra, G. Ramis, G. Busca, Appl. Catal. A 107 (1994) 249.
[8] L.R. Pizzo, C.V. Cáceres, M.N. Blanco, Catal. Lett. 33 (1995) 175–192.
[9] D. Kim, M. Ostromecki, I.E. Wachs, D. Kohler, J.G. Eckerdt, Catal. Lett. 33 (1995) 209.
[10] J. Leyrer, R. Margraf, E. Taglauer, H. Knözinger, Surf. Sci. 201 (1988) 603.
[11] A. Baiker, P. Dollenmeier, M. Glinski, A. Reller, Appl. Catal. 35 (1987) 351.
[12] A. Baiker, P. Dollenmeier, M. Glinski, A. Reller, Appl. Catal. 35 (1987) 365.
[13] M. Schraml, W. Fluhr, A. Wokaun, A. Baiker, Ber. Bunsenges. Phys. Chem. 93 (1989) 852.
[14] B.E. Handy, M. Maciejewski, A. Baiker, J. Catal. 134 (1992) 75.
[15] U. Scharf, M. Schraml-Marth, A. Wokaun, A. Baiker, J. Chem. Soc. Faraday Trans. 87 (19) (1991) 3299.
[16] J. Engweiler, A. Baiker, Appl. Catal. A 120 (1) (1994) 187.
[17] J.M. Stencel, Raman Spectroscopy for Catalysts, Van Nostrand Reinhold, New York, 1990.
[18] W.P. Griffith, P.J.B. Lesniak, J. Chem. Soc. A (1961) 1066.
[19] E. Salje, Acta Cryst. A 31 (1975) 360.
[20] M.F. Daniel, B. Desbat, J.C. Lassegues, R.J. Garie, Solid State Chem. 67 (1987) 235.
[21] G. Busca, G. Ramis, J.M.G. Amores, V.S. Escribano, P. Piaggio, J. Chem. Soc. Faraday Trans. 90 (20) (1994) 3181.
[22] E. Payen, S. Kasztelan, J. Grimblot, J.P. Bonelle, J. Raman Spectrosc. 17 (1986) 233.
[23] S.S. Chan, I.E. Wachs, L.L. Murell, L. Wang, W.K. Hall, J. Phys. Chem. 88 (1984) 5831.
[24] K. Jagannathan, A. Srinivasan, C.N.R. Rao, J. Catal. 69 (1981) 418–427.
[25] D.C. Vermaire, P.C. van Berge, J. Catal. 116 (1989) 309–317.
[26] J.N. Fiedor, A. Proctor, M. Houalla, D.M. Hercules, Surf. Interface Anal. 23 (1995) 204.
[27] J. Engweiler, Titania based vanadia, chromia and tungsten oxide catalysts prepared by grafting, PhD thesis, ETHZ, 1995.
[28] G.T. Went, L.-J. Leu, A.T. Bell, J. Catal. 134 (1992) 479.
[29] J.F. Moulder, W.F. Stickle, P.E. Sobol, K.D. Bomben, in: J. Chastain (Ed.), Handbook of X-ray Photoelectron Spectroscopy, Perkin-Elmer, Eden Prairie, MN, 1992.
[30] J.H. Scofield, J. Electron. Spectrosc. Relat. Phenom. 8 (1976) 129.
[31] G. Ramis, G. Busca, C. Cristiani, L. Lietti, P. Forzatti, F. Bregani, Langmuir 8 (1992) 1744.
[32] G. Oliveri, G. Ramis, G. Busca, V.S. Escribano, J. Mater. Chem. 3 (12) (1993) 1239.
[33] M.P. Seah, in: D. Briggs, M.P. Seah (Eds.), Practical Surface Analysis, Vol. 1, Chap. 5, Wiley, 1994.
[34] D.R. Penn, Phys. Rew. B 13 (1976) 5243.
[35] G.C. Bond, S. Flamerz, L. van Wijk, Catal. Today 1 (1987) 229.
[36] M.A. Vuurman, I.E. Wachs, A.M. Hirt, J. Phys. Chem. 95 (1991) 9928.
[37] C.F. Baes, Jr., R.E. Mesmer, The Hydrolysis of Cations, Wiley, New York, 1986.
[38] S.S. Chan, I.E. Wachs, L.L. Murrell, N.C. Dispenziere, in: S. Kaliaguine, A. Mahay (Eds.), Catalysis on the Energy Scene, Elsevier, 1984, p. 259.